Inorganic Chemistry Communications 162 (2024) 112272

Contents lists available at ScienceDirect

Inorganic Chemistry Communications

journal homepage: www.elsevier.com/locate/inoche

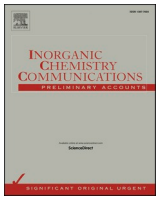

Short communication

Photocatalytic degradation of methyl orange using CuO/Al_2O_3 nanocomposite obtained by microwave-assisted thermal decomposition route

Hanan Alhussain [a], Hela Ferjani [a,*], Opeyemi A. Oyewo [b], Seshibe Makgato [b], Damian C. Onwudiwe [c,d,*]

[a] Chemistry Department, College of Science, Imam Mohammad Ibn Saud Islamic University (IMSIU), Riyadh 11623, Saudi Arabia
[b] Department of Chemical Engineering, College of Science, Engineering and Technology, University of South Africa (UNISA), c/o Christian de Wet &Pioneer Avenue, Florida Campus 1710, Johannesburg, South Africa
[c] Materials Science Innovation and Modelling (MaSIM) Research Focus Area, Faculty of Natural and Agricultural Science, North-West University (Mafikeng Campus), Mmabatho, South Africa
[d] Department of Chemistry, Faculty of Natural and Agricultural, Science, North-West University (Mafikeng Campus), Private Bag X2046, Mmabatho 2735, South Africa

ARTICLE INFO

Keywords:
Alumina
Copper oxide
Structural properties
Morphology
Microwave irradiation

ABSTRACT

Aluminum oxide (Al_2O_3) and copper oxide (CuO) are known to exhibit very exceptional properties including high thermal and chemical properties that promise a wide area of applications. In this paper, we report the microwave-assisted thermal decomposition route to CuO/Al_2O_3 nanocomposite and its application as a photocatalyst for methyl orange (MO) degradation. Al_2O_3 was first prepared at different temperatures of 900, 1000, and 1100 °C, denoted as Al_2O_3(1), Al_2O_3(2), and Al_2O_3(3). Subsequently, the best temperature (1000 °C) was selected for the synthesis of CuO/Al_2O_3 nanocomposite. XRD analysis confirmed the hexagonal crystal structure for all the Al_2O_3 and the monoclinic phase for the CuO within the composite. The crystallite sizes of the alumina increased with temperature and a similar growth pattern occurred in the entire samples. Scanning electron microscopy and transmission electron microscopy (SEM and TEM) show clear spherical morphology for all the samples with obvious agglomeration as temperature increases. Optical characterization displayed decreasing band gap energies with increasing temperature, implying size increase due to particle interaction, boundary energy reduction, and grain boundary migration. The photocatalytic performance of the CuO/Al_2O_3 under visible light was evaluated on methyl orange (MO), and the degradation was studied with some process parameters such as the effect of catalysts dosage and initial concentration of MO. Results showed that the CuO/Al_2O_3 exhibited about 94.2 % efficiency within 3 h using an optimum dose of 2.0 g/L and an initial MO concentration of 20 mg/L. However, the use of CuO/Al_2O_3 nanocomposites to remove other organic pollutants could confirm the robustness of this catalyst.

1. Introduction

The release of hazardous waste, particularly from textile and other chemical industries, into water streams poses significant risks to both the environment and human health. These wastes often contain toxic substances and chemicals that are harmful and non-biodegradable [1]. Dyes represent one of the most perilous contaminants found in water sources. Within the industrial sector, textile processes including dyeing, printing, finishing, and washing account for 85 % of total water usage and 65 % of chemical consumption in the textile supply chain [2]. Approximately 7.5 metric tons of pollutants are discharged annually solely from dyeing processes. The intricate molecular structures of dyes, consisting of aromatic rings linked with various functional groups carrying π-electrons, enable them to absorb light within the 380–700 nm spectra, resulting in coloration owing to the presence of chromogens and chromophores. Among both natural and synthetic dyes, the prevalence of azo compounds has raised concerns due to their highly carcinogenic nature, primarily emanating from amine and benzidine emissions.

* Corresponding authors at: Materials Science Innovation and Modelling (MaSIM) Research Focus Area, Faculty of Natural and Agricultural Science, North-West University (Mafikeng Campus), Mmabatho, South Africa (D.C. Onwudiwe).
E-mail addresses: hhferjani@imamu.edu.sa (H. Ferjani), Damian.Onwudiwe@nwu.ac.za (D.C. Onwudiwe).

https://doi.org/10.1016/j.inoche.2024.112272
Received 15 December 2023; Received in revised form 23 February 2024; Accepted 6 March 2024
Available online 7 March 2024

Moreover, the non-biodegradable nature of dye molecules contributes to their prolonged persistence in the environment, escalating associated hazards [3].

Methyl orange, also known as dimethylaminoazobenzenesulfonate, is a prevalent azo-anionic dye. This synthetic organic dye is soluble in water, demonstrates remarkable color intensity, and exhibits a vibrant orange colour upon dissolution in water [4]. Typical of all Azo dyes, methyl orange is known to be a major human carcinogen apart from being a water pollutant. Its presence in the environment remains a cause for concern especially in the developing nations where their usage seems to be unrestricted. Hence, the need to remove methyl orange from aqueous systems continues to generate research interest. Different methods of MO removal have been reported such as coagulation-flocculation ultra-filtration [5,6], electrochemical degradation [7,8], and advanced oxidation processes such as non-thermal plasma advanced oxidation process [9], and photocatalytic degradation [10–14]. One of the critical factors considered in the adoption of pollutant removal methods is cost efficiency and complete mineralization of pollutants. To this end, photocatalytic degradation of waste presents significant potential as a sustainable and effective oxidation method, particularly in the field of wastewater treatment [15]. The low operational expenses, rapid mineralization of specific pollutants, and the absence of the necessity for high pressure and temperature make photocatalytic oxidation particularly advantageous [16].

Semiconductor metal oxides have been widely utilized as photocatalysts in dye degradation [17–19] and due to the challenges of the recombination process, the use of heterojunction systems has been considered one of the ways to address this shortcoming [20,21]. The compatibility of the electronic structure of the compositing semiconductor materials is very important, hence TiO_2@ZnO [22], CuO/CeO_2 [23], SnO_2–ZnO [24], Fe_2O_3/γ-Al_2O_3 [25], Ag_2O/MoS_2 [26], WO_4/TiO_2 [27], Fe_2O_3 on NCQDs–MgO [28], GO on Mn_3O_4/TiO_2 [29], Bi_2O_3 QDs on TiO_2 [30], Cu_2O-$BiVO_4$-WO_3 [31], and Fe/ZnO/SiO_2 [32] nanostructured photocatalysts have been reported for water remediation. Alumina coupled to other metal oxide nanoparticles has been used as heterojunction photocatalyst system [33–36]. The combination of CuO and Al_2O_3 proves effective in eliminating pollutants because of the low conductivity, high surface area, low dielectric constant, low thermal expansion, and chemical stability associated with the composite [37–39]. Furthermore, Al_2O_3 showcases an abundance of defect sites, which not only positions it as an exceptional electron acceptor but also significantly bolsters overall efficiency as a photocatalyst to remove dyes from aqueous system [39,40]. In this context, CuO/Al_2O_3 nanocomposites prepared by different processes have been reported. For example, Sridevi *et al* prepared CuO/Al_2O_3 by hydrothermal treatment for enhanced visible-light driven photocatalytic activity [41], sol–gel method has been adopted by Marulasiddeshi *et al* to prepare CuO/Al_2O_3 [42], and the pressureless sintering method using CuO and calcined white Al_2O_3 have also been reported [43]. CuO/Al_2O_3 and ternary composites such as CuO/CeO_2-Al_2O_3, and CuO/La_2O_3-Al_2O_3 catalysts have been prepared by an impregnation method [44]. Al_2O_3:CuO synthesized by the polymeric precursor method by varying the pH of the precursor solution has been presented [45].

Microwave irradiation synthesis method is one of the approaches used for the preparation of metal oxide [46,47] and complex metal oxide nanoparticles [48,49]. The generated microwave impacts reaction processes due to its ability to generate high-frequency waves that heat up reactants within a short time. Similarly, calcination temperature influences the structure, morphology, and particle size of the nanomaterials. In this current study, Al_2O_3/CuO nanocomposite was synthesized by microwave-assisted thermal decomposition route and its application in the degradation of methyl orange was evaluated.

2. Experimental

2.1. Materials

Analytical grades of aluminum acetate, zinc acetate, ethylene glycol, methyl orange, NaOH and HCl (32 %), were purchased from Merck. They were used as received without additional purification.

2.2. Characterization techniques

X-ray powder diffractometer was recorded at room temperature in conjunction with a CuKα ($\lambda = 1.5406$ Å) to measure the diffraction patterns. Morphological analysis of the samples was measured using a JEOL 5600LV scanning electron microscope (SEM) and Hitachi HF–2000 transmission electron micrographs (TEM). Prove 300 UV–vis spectrophotometer was used for the measurement of the Absorption spectroscopy.

2.3. Method of synthesis

The synthesis of Al_2O_3 and CuO/Al_2O_3 was conducted according to the following procedure: Firstly, 1.5 g of aluminium acetate was dispersed in 25 mL ethylene glycol and the solution was thoroughly stirred at 40 °C for 1 h. This was followed by a dropwise addition of 1 M sodium hydroxide to adjust the pH of the stirred solution to 10. The solution was subsequently poured into a microwave vessel lined with PTFE and resistant to pressure, where it was allowed to undergo a reaction through cyclic microwave radiation at 800 W. After 5 min, the microwave heating was stopped, and the solution was cooled to ambient temperature and centrifuged. The resulting precipitate was rinsed thrice with ethanol and left to air dry. Finally, the product was divided into 3 portions and each portion was transferred to a crucible and calcinated in a furnace for 2 h at different temperatures of 900, 1000, and 1100 °C.

CuO/Al_2O_3 nanocomposite was prepared by mixing an equal amount of aluminium acetate and copper acetate (0.5 g) dissolved in 20 mL ethylene glycol and vigorously stirred at 40 °C for 1 h. A solution of 1 M sodium hydroxide was added in dropwise to the mixture to adjust the pH to 10 and the solution was then poured into a microwave vessel lined with PTFE and resistant to pressure, where it was allowed to undergo a reaction through cyclic microwave radiation at 800 W. The microwave heating was stopped after 5 min and the solution was to cool to ambient temperature and centrifuged. The resulting precipitate was rinsed thrice with ethanol and left to air dry. Finally, the product was transferred to a crucible and calcinated in a furnace for 2 h at 1000 °C.

2.4. Photocatalysis studies

The photocatalytic activity of the synthesized CuO/Al_2O_3 nanocomposite was evaluated by studying its photocatalytic potency on an aqueous solution of MO under visible light irradiation. The photocatalytic reactor is equipped with a 250-W Xe discharge lamp and a reactor vessel which has an inbuilt recirculating water source. The vessel was charged with a specific dye solution and a known concentration of catalyst. The photocatalytic experiment proceeds with stirring the mixture of the dye solution and catalyst in the dark for about 20–30 min to allow equilibration, followed by the irradiation by the light from the Xenon lamp. During this process, the solution was constantly agitated under the lamp and aliquots were drawn from the system every 15 min, filtered and measure using UV–visible spectroscopy. This process was allowed to run over a period of 3 h [13].

3. Results and discussion

3.1. XRD studies

X-ray diffraction patterns of the Al_2O_3 nanoparticles calcinated at

900, 1000, and 1100 °C are depicted in Fig. 1a-c, and demonstrates a successful synthesis of the nanoparticles. Similar patterns occurred in the three samples prepared at different calcination times. However, the XRD results also exhibit the effect of calcination time on the crystallinity and crystal size.

The sample calcined at 900 °C (Fig. 1 (a)) displays low intensities peaks which are relatively broad and are attributed to the (012), (104), (110), (113), (024), (116), (211), (018), (214), (300), (1010), (220), (223), (312), and (0210) of α-Al_2O_3 and corresponds to JCPDS file no. 71–1123 with space group $R\bar{3}c$ [50]. It can be observed that a more crystalline phase of α-Al_2O_3 phase is formed after 1000 °C as presented in Fig. 1 (b and c). The samples prepared at 1000 and 1100 °C

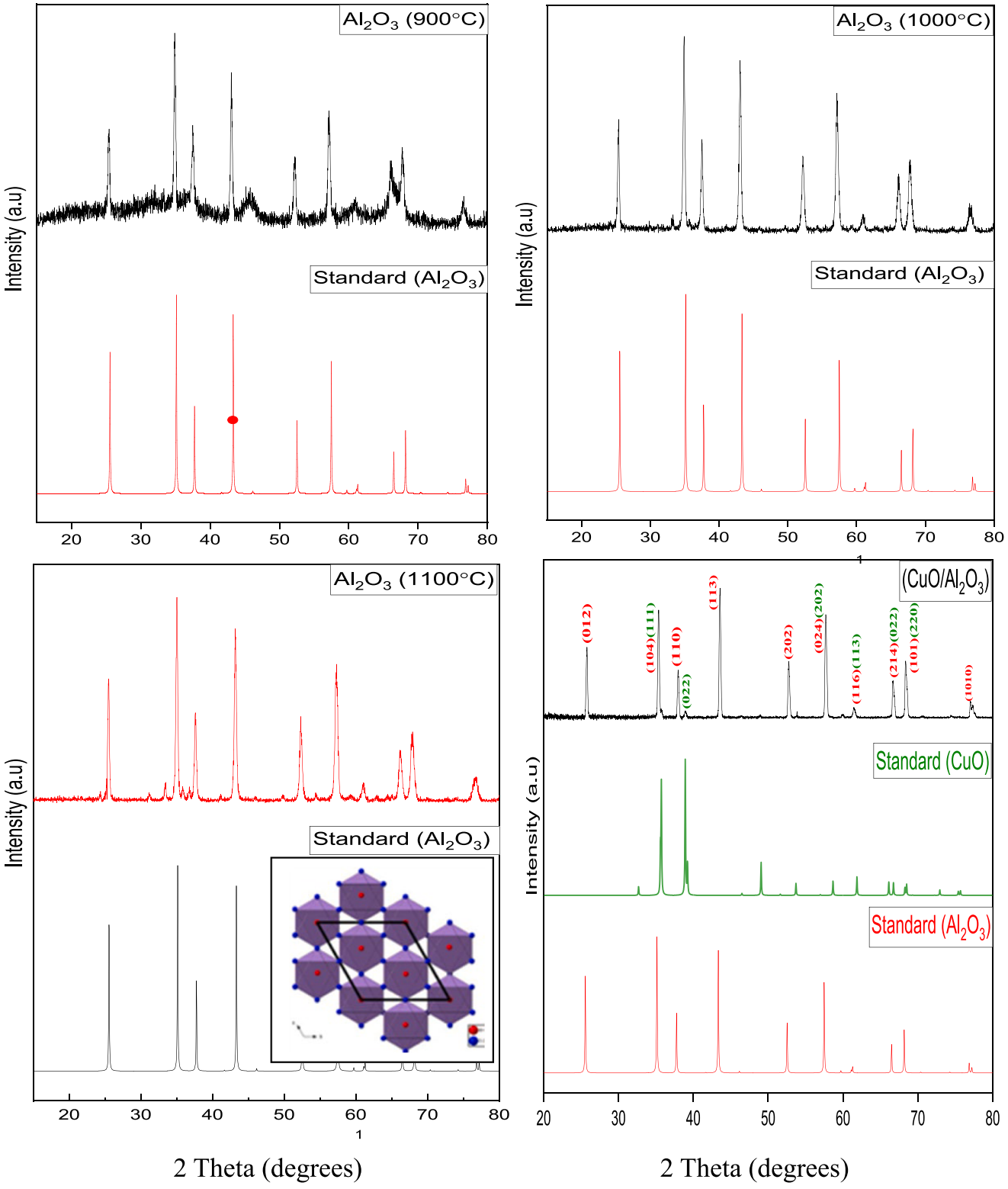

Fig. 1. XRD patterns of Al_2O_3 NPs synthesized at different calcination temperatures of (a) 900, (b) 1000, and (c) 1100 °C (inset is the packing diagram of α-Al_2O_3 nanoparticles). (d) XRD patterns of CuO/Al_2O_3.

have more intense and narrower peaks that suggest larger crystal sizes. Beyond 1000 °C, the Al_2O_3 samples not only increased in crystallite size as indicated in the sharp peaks, but also a reduction in the background noise occurred. α phase of Al_2O_3 is the most stable form and has been reported to be formed only at temperatures beyond 1000 °C. The formation of this phase at 900 °C could be related to the synthesis procedure, which is different from other reported processes involving a combustion agent such as citric acid [51–53].

The diffraction patterns of the CuO/Al_2O_3 nanocomposite show that the sample has been obtained from two components of CuO and Al_2O_3. The diffraction peaks due to the CuO could be identified at 2θ of 35.63, 38.80, 53.34, 58.23, 61.62, and 66.35, which are assigned to the (1 1 1), (0 2 2), (0 2 0), (2 0 2), (1 1 3), and (2 2 0) planes of monoclinic CuO (JCPDS 45–0397), and patterns ascribed to the Al_2O_3 agree very well with the hexagonal α-alumina phase. There was no change in the crystalline phase of the alumina emanating from the incorporation of a secondary semiconductor metal oxide to form a composite system. CuO/Al_2O_3 nanocomposite synthesized by the conventional methods [54,55], also indicated the formation of the monoclinic phase for the CuO. However, γ-Al_2O_3 crystalline phase was reported with standard alumina card (JCPDS files no. 29.0063) and JCPDS No. 10–425) respectively.

The average crystalline size was estimated using the Scherrer equation (1)[56]. where D is the average crystal size, K is known as Debye–Scherrer's constant, and it is given as 0.89 for spherically shaped samples, λ denotes the X-ray radiation wavelength (often given as $\lambda =$ 1.54 for CuKα Å, β is the width of the peak at half-maximum intensity (FWHM) of the sample (radian) and θ is the diffraction angle [57,58]. The estimated crystalline sizes of 45.2, 48.4 and 56.8 nm for Al_2O_3 (1), Al_2O_3 (2), and Al_2O_3 (3) are in line with the crystal growth that takes place with temperature.

3.2. Morphological analysis

Fig. 2(a–c) present the external morphology of the Al_2O_3 nanoparticles synthesized at different temperatures, 900, 1000, and 1100 °C respectively. The SEM images show particles with nearly spherical shapes and agglomeration with no distinct edge. The micrographs show that temperature increases the agglomeration, causing the particles to form crumps at 1100 °C. The temperature change leads to significant morphological changes in the structure of the nanoparticles. With enhanced calcination temperatures, a variation occurs in the size and shape of the nanoparticles and increased agglomeration may also be due to the improved surface forces among the particles [59]. Larger particles and large pores have been located at different agglomeration junctions [60].

The transmission electron microscopy images (Fig. 3) give NPs of similar shape and the size estimation using image J shows sizes of 42.8, 44.4 and 58.5 nm for the samples obtained at 900, 1000 and 1100 °C respectively. These are close to the sizes calculated from their XRD patterns and it could be observed that apart from the size increment, agglomeration of the particles increases as the temperature increase which has been attributed to surface reactivity.

The surface morphology of the composite has been visualized using Scanning Electron Micrographs (SEM) and presented in Fig. 4a. From the figure, the external surface morphology of the CuO/Al_2O_3 nanoparticles depict spherical morphology with a slight agglomeration of nanoparticles that is expected for such a high-temperature calcination process. TEM images of CuO/Al_2O_3 show spherical morphology whose average particle size is about 52.4 nm, and this agrees well with the calculated crystallite size using Scherrer's equation. The HR-TEM images are depicted in Fig. 4(c), showing lattice fringes with interplanar spacing of 0.23 and 0.26 nm corresponding to (1 1 0) and (−1 1 1) planes of Al_2O_3 and CuO, respectively [61,62]. Both the XRD and EDX (presented in Fig. 4c) analyses were confirmatory of the successful formation of a pure phase composite of CuO/Al_2O_3.

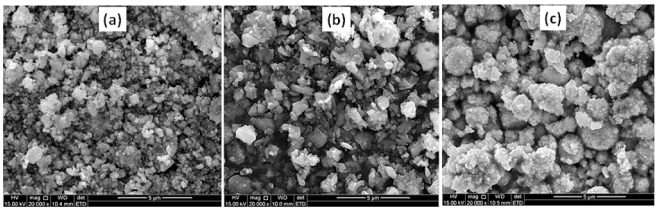

Fig. 2. SEM micrographs of Al_2O_3 NPs synthesized at different calcination temperatures of (a) 600, (b) 800, and (c) 1000 °C.

3.3. Optical absorption properties

The UV–Vis spectra of the different samples of the γ-Al_2O_3 NPs and the composite with CuO are shown in Fig. 5(a-d). The sharp absorption edge exhibited by all the spectra around 280 nm is ascribed to the photoexcitation of electrons causing migration from the valence band to the conduction band [63]. In addition, the absorption spectrum of CuO/Al_2O_3 nanocomposite (Fig. 6d) shows a broad absorption band in the spectral range of 385 to 410 nm attributed to the photoexcitation of electrons in the CuO.

The optical band gap of the Al_2O_3 nanoparticles at varying calcination temperatures has been calculated using the Tauc relation given in Equation 1 [64]:

$$(h\nu\alpha) = (h\nu - Eg)^n \quad (1)$$

where α represents the absorption coefficient, ν denotes the frequency, h is the Planck's constant, Eg is the value for the absorption band gap energy and n is a constant that is related to the different types of electronic transitions whereby the direct allowed, indirect allowed, direct forbidden, indirect forbidden transitions are associated with n = 1/2, 2, 3/2 or 3 respectively).

The linear part of the $(\alpha h\upsilon)^2$ vs photon energy (hυ) curves is shown in Fig. 6. The values of the band gap decreased from 4.4 to 3.8 eV with increasing calcination temperature from 900 to 1100 °C. The existence of impurities and structural default like oxygen vacancies and interstitials could influence the measurements of the energy band gap. Therefore, the decrease in band gap values could be due to the diffusion of aluminum and oxygen atoms that occupy interstitial sites between Al_2O_3 lattices, which resulted in the decrease in the band gap energies. The band gap energy of the composite was obtained as 4.3 eV. Table 1 summarises the values of the optical band gap of the Al_2O_3 nanoparticles for varying calcination temperatures (900, 1000, and 1100 °C).

3.4. Photodegradation of methyl orange

The generation of conduction band electrons (e•) and valence band holes (h^+) upon the irradiation of CuO/Al_2O_3 nanocomposite is significant for the degradation of the methyl orange. The photo-generated electrons could react with electron acceptors such as O_2, adsorbed on the surface of the catalyst to form a superoxide radical anion O_2•. Concomitantly, photogenerated holes oxidize the organic molecules and react with OH. or H_2O which oxidizes them into OH• radicals. The generated radicals together with other highly oxidant species (peroxide radicals) are responsible for the photodecomposition of MO into less harmful mineral end-products [65]. The recombination of electron-hole pairs has the potential to generate energy through fluorescence emission. Nevertheless, a reduced emission intensity extends the duration of electron-hole recombination and promotes the rate of photocatalytic activity. [66,67]. Therefore, using a 250–W Xe lamp as an excitation source for the heterogeneous CuO/Al_2O_3, electrons and holes could have a longer lifetime and may form a higher number of active radicals [10,66]. Fig. 6 illustrates the absorption spectra depicting the degradation of MO at 15-minute intervals under visible light. The findings

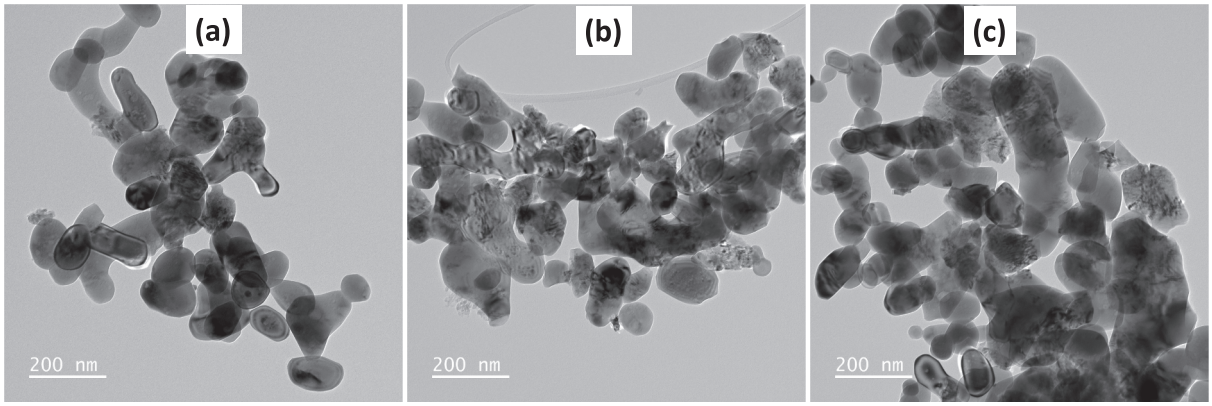

Fig. 3. TEM micrographs of Al_2O_3 NPs synthesized at different calcination temperatures of (a) 900, (b) 1000, and (c) 1100 °C.

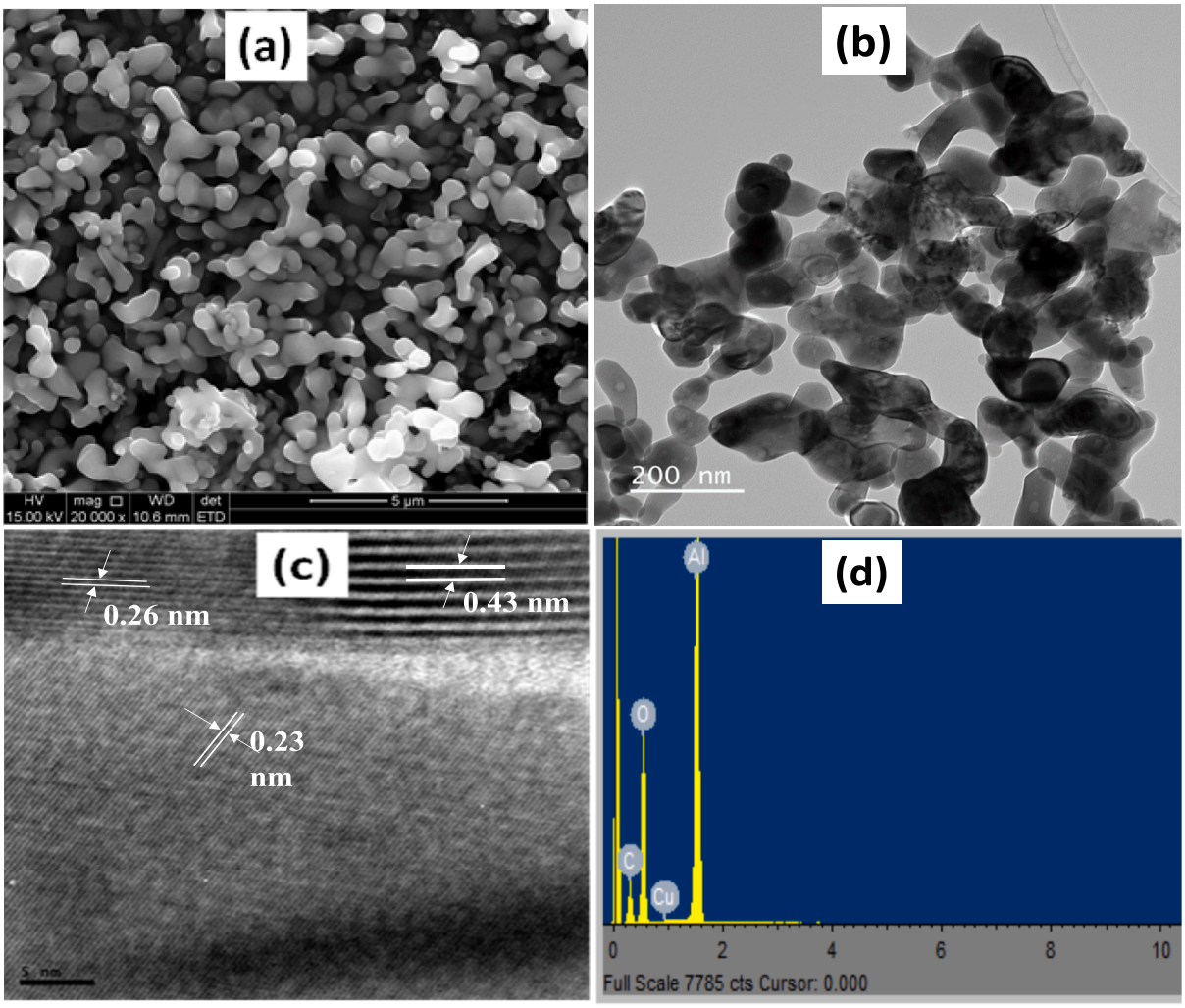

Fig. 4. (a) SEM, (b) TEM, and (c) HRTEM micrographs of CuO/Al_2O_3.

indicate a gradual decline in the absorption peak of MO at approximately 430 nm. Effective MO degradation (94 %) was accomplished within a 3-h reaction time utilizing a combination of 2.0 g/L CuO/Al_2O_3 and 20 mg/L MO concentration. Comparable outcomes have been reported in prior studies [68,69].

The performance of CuO/Al_2O_3 nanocomposite was compared with other studies involving Al_2O_3 composite with similar II-VI semiconductor photocatalysts. For example, $MgO•Al_2O_3•ZnO$ composite, synthesized by the coprecipitation of their carbonates and evaluated for the photocatalytic degradation of methyl violet 6b exhibited a degradation efficiency of 48.7 %. Only upon the addition of H_2O_2 was the efficiency increased to 93.42 % at pH 9 [70]. The visible light activated photocatalytic performance of $CdO\text{-}Al_2O_3$ nanocomposite has been studied against metanil yellow dy. A maximum degradation

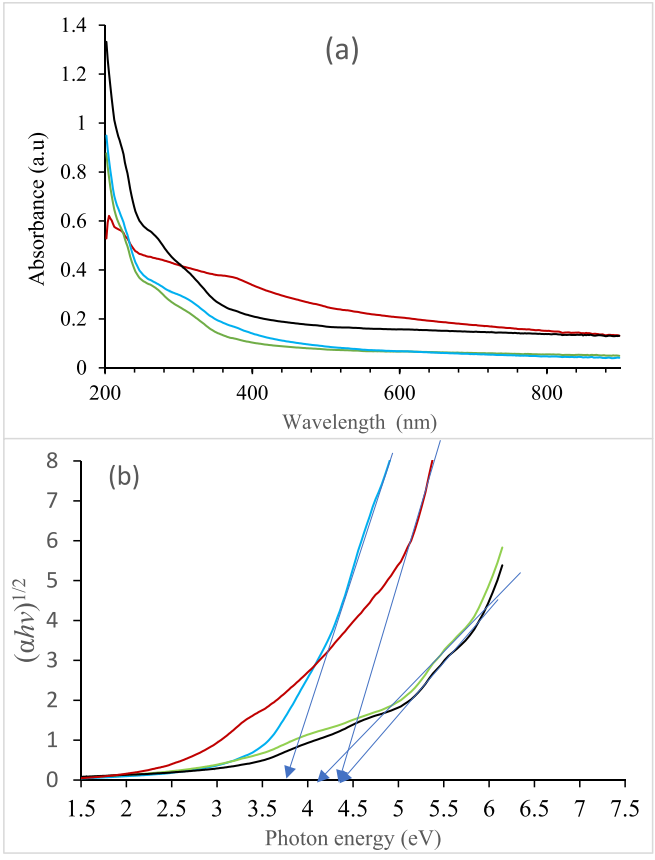

Fig. 5. (a) Absorption spectra and (b) Tauc plot of Al_2O_3 NPs synthesized at different calcination temperatures of 900, 1000, and 1100 °C. Black: Al_2O_3(900); green: Al_2O_3(1000); blue: Al_2O_3(1100); red: CuO/Al_2O_3. (For interpretation of the references to color in this figure legend, the reader is referred to the web version of this article.)

efficiency of 82.09 % was achieved [71]. Nanocomposites of mixed iron and aluminium oxide (Fe_2O_3–Al_2O_3) have been used for the adsorptive decolorization of Congo red dye from an aqueous system [72]. Anatase phase of TiO_2 nanoparticles were incorporated into alumina to form TiO_2/Al_2O_3 composites. They were evaluated for the photocatalytic removal of methylene blue (MB) and crystal violet (CV) dyes under both UV- and visible light. The degradation efficiency was 45 and 29 % under the UV light and 84 and 81 % under visible light for MB and CV dyes respectively [73]. Yadav et al [40], reported the photocatalytic activity of ZnO/Al_2O_3 nano-composites using cibacron red dye. The photocatalytic efficiency of different compositional ratios were investigated and the highest recorded efficiency was 74.89 % [40].

3.5. Effect of solution pH and photocatalysts dosage

The solution pH and amount of photocatalyst used for the degradation process are some of the critical parameters in the assessment of the degradation efficiency of dyes. Therefore, the influence of the pH of the solution was assessed in the range 3–9, and the results are presented in Fig. 7a. It shows that the degradation of the dye was highest in the acidic range of the solution (pH3) compared to the alkaline range. Similarly, the effect of the photocatalyst dosage was studied by varying the concentration of CuO/Al_2O_3 from 0.5 to 2.5 g/L, was studied on the degradation of 20 mg/L MO concentration at pH = 3. The result presented in Fig. 7b display an insignificant increase in the degradation of MO in the absence of CuO/Al_2O_3, confirming that there was no much effect on the degradation of the MO without the catalyst. The efficiency of MO degradation was increased with increasing concentration of the catalyst and the highest results was achieved with the use of 2.5 g/L. This remained almost constant at this high concentration of the catalyst and could be ascribed to the effect of the increased active site on the surface of the photocatalyst as well as improved photo absorption property. Higher amount of CuO/Al_2O_3 implies more active sites that can absorb more photons in the solution. For example, the increase in the catalyst dosage from 0.5 g/L to 2.5 g/L increased the percentage degradation from 46.7 to 94 % after irradiating for 180 min. The

Table 1
Summary of band gap variation with temperature of calcination.

Samples	Temperature (°C)	Band gap energy (eV)
Al_2O_3 (900)	900	3.8
Al_2O_3 (1000)	1000	4.2
Al_2O_3 (1100)	1100	4.4
CuO/Al_2O_3 (1000)	1000	4.3

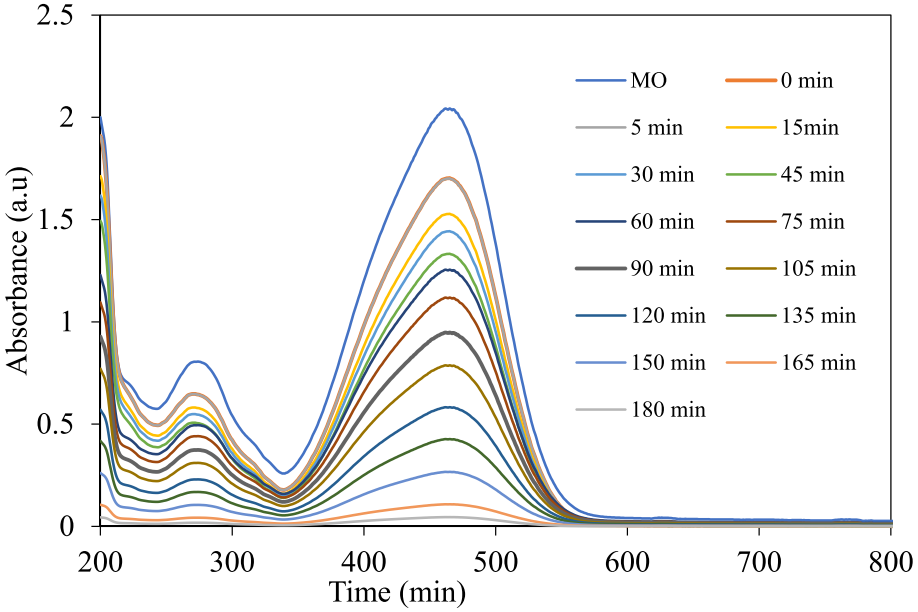

Fig. 6. UV–vis absorption spectra of photocatalytic degradation of MO using CuO/Al_2O_3 nanocomposite.

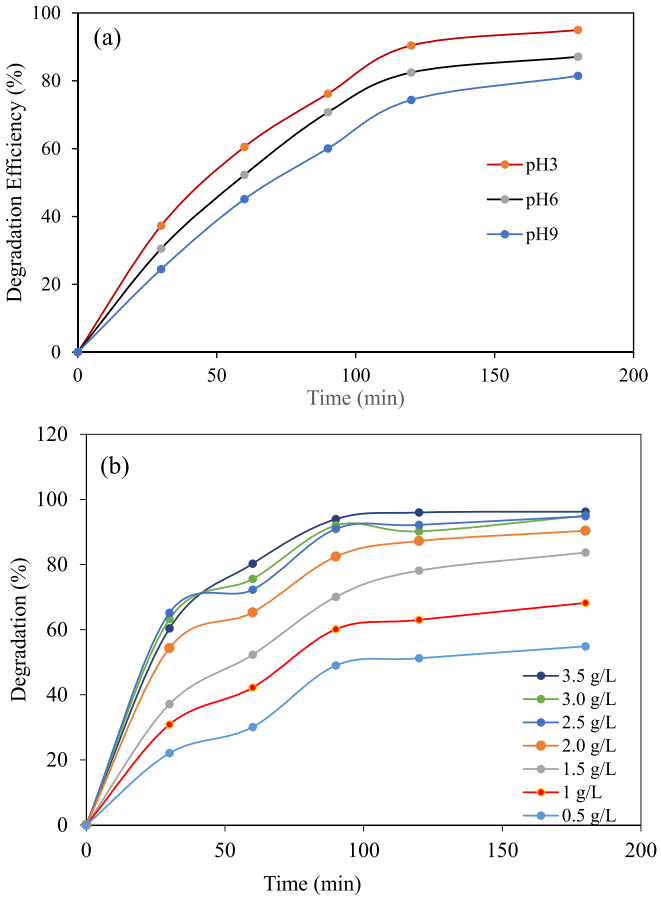

Fig. 7. Effect of CuO/Al_2O_3 nanocomposite loading on the photo enhanced degradation of 20 mg/L solution of MO at the pH: 3.0).

enhanced degradation of MO achieved with 0.25 g/L might be due to the increase in the generation of hydroxyl radicals due to the availability of surface active sites [74]. However, an excessive catalyst dose (above 2.5 g/L) does not display a distinct positive effect on the MO degradation due to the impedance in the light penetration and light scattering by the CuO/Al_2O_3. Subsequently, excess dosage has the tendency to decrease the generation of hydroxyl radicals, and facilitates the agglomeration as well as the sedimentation of the photocatalyst particles in the solution [75]. These results compare reasonably to the results reported for other similar heterojunction photocatalysts [36,76,77].

3.6. *Effects of MO initial concentration*

Methyl orange concentrations ranging from 20 to 110 mg/L were used to establish the effect of the initial MO concentration on the photocatalytic activity of CuO/Al_2O_3 and the result is presented in Fig. 8. The best degradation efficiency of the catalyst on MO was observed at the lowest MO concentration. After 180 min of light irradiation, about 94 % of the dye was photodegraded with the initial concentration of 20 mg/L, while 50, 80 and 110 mg/L reached 80.5, 65.1, 45.3 and 28 % efficiency, respectively. The possible reason might be the visible light screening effect of the MO and the increased formation of hydroxyl radical (•OH) on lower concentration of dye compared to the higher dye concentration [65]. At high concentration of MO, a high absorption of visible light may be absorbed by the MO molecules instead of absorption by CuO/Al_2O_3. Hence, there is a shielding of the incident light by the high concentration of MO, thereby resulting in the impedance of the absorption of light by the CuO/Al_2O_3 catalyst, and this reduces the photocatalytic property of the catalyst [78,79]. Therefore, the efficiency of degradation decreased from 94 to about 28 % when the initial dye

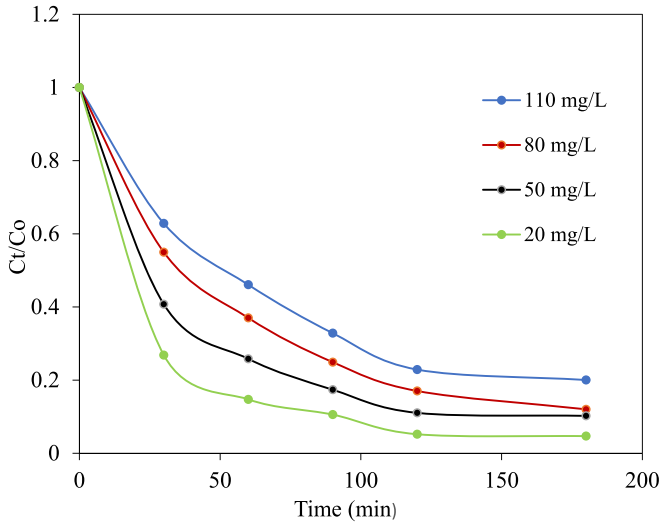

Fig. 8. Effect of initial concentration of MO on its photodegradation using CuO/Al_2O_3 (catalyst dosage: 100 mg and the solution pH: 3.0).

concentration was increased from 20 to 110 mg/L. MO degradation reaches a saturation limit at a lower concentration of the MO because the degradation efficiency increases with decreasing concentration of MO [80]. the results show that photo-enhanced reaction process is dependent on the concentration of the substrate, which is in agreement with other related studies [36,65,81].

To evaluate the recovery cycle of this photocatalyst, experiments were conducted to evaluate its reusability. Fig. 9 illustrates the results of the investigation using 2.5 g/L of the photocatalyst. Even after five consecutive cycles of recyclability assessment, the photocatalyst exhibited above 70 % in activity, suggesting they can be reused at least four times. This gradual decrease in activity with increasing reusability cycles is likely due to the loss of photocatalyst during the separation process.

4. Conclusion

The current study has described a simple approach to the synthesis of semiconductor heterojunction system of CuO/Al_2O_3. The structural properties of the nanocomposite were studied using XRD, while UV–vis spectroscopy was used for the optical characterisation, and SEM, TEM, and HRTEM analytical techniques explored the morphological

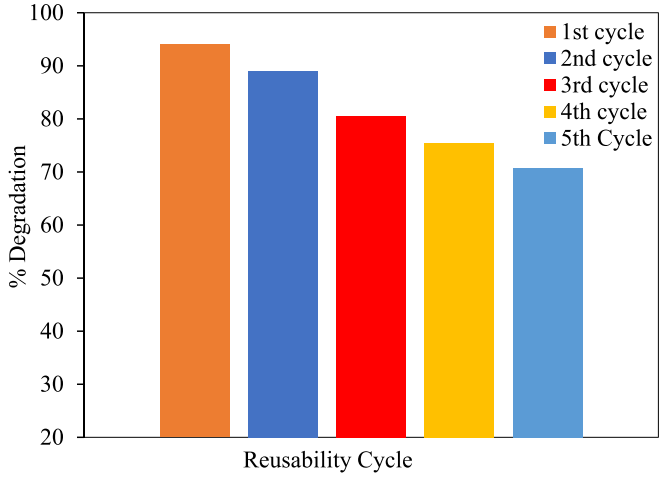

Fig. 9. Reusability cycles of mg/L CuO/Al_2O_3 nanocomposite (catalyst dosage: 2.5 g/L and the solution pH: 3.0).

properties. The absorption spectrum revealed band around 340 nm ascribable to the CuO. Both the SEM and TEM micrographs confirmed agglomerated spherical shaped nanocomposite of CuO/Al_2O_3. The diffraction patterns from the XRD measurement confirmed increased crystallinity of the Al_2O_3 as temperature increased, and subsequent formation of nanocomposite composed of hexagonal Al_2O_3 and monoclinic phase CuO. The crystallite size of the pristine Al_2O_3 was calculated to be 45.2, 48.4 and 56.8 nm. The nanocomposite showed to be effective in degrading methyl orange under visible light irradiation, with over 80 % degradation efficiency reported at the optimal conditions of 2.5 g/L catalyst dosage and 20 mg/L of MO initial concentration. Therefore, this nanocomposite has potential for the degradation of dyes in wastewater and may be further improved to address the challenges of water pollution, which unfortunately has been on the rise. Future research may involve exploring the possibility for large-scale production for application in wastewater treatment plants, the encapsulation of this heterojunction semiconductor photocatalyst into polymeric matrices to ensure the safety of nanomaterials as their usage in addressing several environmental pollution challenges continues to attract attention.

CRediT authorship contribution statement

Hanan Alhussain: Writing – original draft, Resources, Formal analysis. **Hela Ferjani:** Writing – original draft, Formal analysis. **Opeyemi A. Oyewo:** Writing – review & editing, Methodology. **Seshibe Makgato:** Resources. **Damian C. Onwudiwe:** Writing – review & editing, Conceptualization.

Declaration of competing interest

The authors declare that they have no known competing financial interests or personal relationships that could have appeared to influence the work reported in this paper.

Data availability

Data will be made available on request.

Acknowledgment

This work was supported and funded by the Deanship of Scientific Research at Imam Mohammad Ibn Saud Islamic University (IMSIU) (grant number IMSIU-RG23032).

References

[1] M. Mitra, A. Ghosh, A. Mondal, K. Kargupta, S. Ganguly, D. Banerjee, Facile synthesis of aluminium doped zinc oxide-polyaniline hybrids for photoluminescence and enhanced visible-light assisted photo-degradation of organic contaminants, Appl. Surf. Sci. 402 (2017) 418–428.
[2] M.A. Uddin, M.S. Begum, M. Ashraf, A.K. Azad, A.C. Adhikary, M.S. Hossain, Water and chemical consumption in the textile processing industry of Bangladesh, PLOS Sustainability and Transformation 2 (2023) e0000072.
[3] K. Maheshwari, M. Agrawal, A. Gupta, Dye pollution in water and wastewater, Novel Materials for Dye-Containing Wastewater Treatment (2021) 1–25.
[4] L. Wu, X. Liu, G. Lv, R. Zhu, L. Tian, M. Liu, Y. Li, W. Rao, T. Liu, L. Liao, Study on the adsorption properties of methyl orange by natural one-dimensional nano-mineral materials with different structures, Sci. Rep. 11 (2021) 10640.
[5] C.A. Igwegbe, O.D. Onukwuli, J.O. Ighalo, C.J. Umembamalu, Electrocoagulation-flocculation of aquaculture effluent using hybrid iron and aluminium electrodes: a comparative study, Chemical Engineering Journal Advances 6 (2021) 100107.
[6] K.O. Iwuozor, Prospects and challenges of using coagulation-flocculation method in the treatment of effluents, Advanced Journal of Chemistry-Section A 2 (2019) 105–127.
[7] S.-H. Li, Y. Zhao, J. Chu, W.-W. Li, H.-Q. Yu, G. Liu, Electrochemical degradation of methyl orange on Pt–Bi/C nanostructured electrode by a square-wave potential method, Electrochim. Acta 92 (2013) 93–101.
[8] M.M. Islam, S. Basu, Effect of morphology and pH on (photo) electrochemical degradation of methyl orange using TiO2/Ti mesh photocathode under visible light, Journal Of Environmental Chem. Eng. 3 (2015) 2323–2330.
[9] B. Jiang, J. Zheng, Q. Liu, M. Wu, Degradation of azo dye using non-thermal plasma advanced oxidation process in a circulatory airtight reactor system, Chem. Eng. J. 204 (2012) 32–39.
[10] M. Adeel, M. Saeed, I. Khan, M. Muneer, N. Akram, Synthesis and characterization of Co–ZnO and evaluation of its photocatalytic activity for photodegradation of methyl orange, ACS Omega 6 (2021) 1426–1435.
[11] J. Cao, X. Li, H. Lin, B. Xu, S. Chen, Q. Guan, Surface acid etching of (BiO) 2CO3 to construct (BiO) 2CO3/BiOX (X= cl, br, I) heterostructure for methyl orange removal under visible light, Appl. Surf. Sci. 266 (2013) 294–299.
[12] J. Luo, X. Zhou, L. Ma, X. Xu, J. Wu, H. Liang, Enhanced photodegradation activity of methyl orange over Ag2CrO4/SnS2 composites under visible light irradiation, Mater. Res. Bull. 77 (2016) 291–299.
[13] D.C. Onwudiwe, O.C. Olatunde, V.M. Nkwe, Y. Ben Smida, H. Ferjani, Dual S-scheme heterojunction g-C3N4/Bi2S3/CuS composite with enhanced photocatalytic activity for methyl orange degradation, Inorg. Chem. Commun. 155 (2023) 111075.
[14] D.C. Onwudiwe, V.M. Nkwe, O.C. Olatunde, H. Ferjani, Graphitic carbon nitride functionalized with cu-doped Bi2S3 as a heterostructure photocatalyst for the visible light degradation of methyl orange, Ceram. Int. 49 (2023) 19451–19462.
[15] G. Ren, H. Han, Y. Wang, S. Liu, J. Zhao, X. Meng, Z. Li, Recent advances of photocatalytic application in water treatment: a review, Nanomaterials (basel) 11 (2021).
[16] S. Kumar, W. Ahlawat, G. Bhanjana, S. Heydarifard, M.M. Nazhad, N. Dilbaghi, Nanotechnology-based water treatment strategies, J. Nanosci. Nanotechnol. 14 (2014) 1838–1858.
[17] N.T.H. Giang, N.T. Thinh, N.D. Hai, P.T. Loc, T.N.A. Thu, N.H.P. Loan, D.M. Quang, L.D. Anh, V.N.T. Truong An, M.T. Phong, N.H. Hieu, Application of TiO2 nanoparticles with natural chlorophyll as the catalyst for visible light photocatalytic degradation of methyl orange and antibacterial, Inorg. Chem. Commun. 150 (2023) 110513.
[18] F. Khan, Statistical applications for photocatalytic dye degradation and sorption models study assess by Co3O4 nanoadsorbent, Mater. Today Chem. 17 (2020) 100330.
[19] D.C.T. Nguyen, W.-C. Oh, Ternary self-assembly method of mesoporous silica and Cu2O combined graphene composite by nonionic surfactant and photocatalytic degradation of cationic-anionic dye pollutants, Sep. Purif. Technol. 190 (2018) 77–89.
[20] S. Xue, C. Wu, S. Pu, Y. Hou, T. Tong, G. Yang, Z. Qin, Z. Wang, J. Bao, Direct Z-scheme charge transfer in heterostructured MoO3/g-C3N4 photocatalysts and the generation of active radicals in photocatalytic dye degradations, Environ. Pollut. 250 (2019) 338–345.
[21] C. Li, G. Zhao, T. Yan, T. Zhang, X. Liu, X. Long, H. Duan, F. Jiao, Enhanced visible-light-induced photocatalytic performance of Bi2O3/ZnAl-LDH–C for dyes removal in water, Mater. Lett. 244 (2019) 215–218.
[22] H.M. Mousa, J.F. Alenezi, I.M.A. Mohamed, A.S. Yasin, A.-F.-M. Hashem, A. Abdal-hay, Synthesis of TiO2@ZnO heterojunction for dye photodegradation and wastewater treatment, J. Alloy. Compd. 886 (2021) 161169.
[23] D. Xu, F. Cheng, Q. Lu, P. Dai, Microwave enhanced catalytic degradation of methyl Orange in aqueous solution over CuO/CeO2 catalyst in the absence and presence of H2O2, Ind. Eng. Chem. Res. 53 (2014) 2625–2632.
[24] M.T. Uddin, Y. Nicolas, C. Olivier, T. Toupance, L. Servant, M.M. Müller, H.-J. Kleebe, J. Ziegler, W. Jaegermann, Nanostructured SnO2–ZnO heterojunction photocatalysts showing enhanced photocatalytic activity for the degradation of organic dyes, Inorg. Chem. 51 (2012) 7764–7773.
[25] Y. Liu, D. Sun, Effect of CeO2 doping on catalytic activity of Fe2O3/γ-Al2O3 catalyst for catalytic wet peroxide oxidation of azo dyes, J. Hazard. Mater. 143 (2007) 448–454.
[26] N.R. Khalid, M. Bilal, M.B. Tahir, M. Shakil, T. Iqbal, M. Rafique, N. Yousaf, S.S. A. Gillani, Interfacial coupling effect of Ag2O nanorods over MoS2 microflowers for improved photocatalytic activity, Ceram. Int. 46 (2020) 6856–6859.
[27] A.K.L. Sajjad, S. Shamaila, J. Zhang, Tungstate/titanate composite nanorod as an efficient visible light photo catalyst, J. Hazard. Mater. 235–236 (2012) 307–315.
[28] G.S. Jamila, S. Sajjad, S.A.K. Leghari, M. Mehboob, C. Flox, Enhanced electron transport by Fe2O3 on NCQDs–MgO nanostructure for solar photocatalysis and electrocatalytic water splitting, Applied Nanoscience 12 (2022) 1815–1827.
[29] S. Noor, S. Sajjad, S.A.K. Leghari, C. Flox, T. Kallio, E.I. Kauppinen, S. Ahmad, Electronic transitions of SWCNTs in comparison to GO on Mn3O4/TiO2 nanocomposites for hydrogen energy generation and solar photocatalysis, New J. Chem. 45 (2021) 2431–2442.
[30] S. Noor, S. Sajjad, S.A.K. Leghari, C. Flox, S. Ahmad, Competitive role of nitrogen functionalities of N doped GO and sensitizing effect of Bi2O3 QDs on TiO2 for water remediation, J. Environ. Sci. 108 (2021) 107–119.
[31] N. Omrani, A. Nezamzadeh-Ejhieh, A comprehensive study on the enhanced photocatalytic activity of Cu2O/BiVO4/WO3 nanoparticles, J. Photochem. Photobiol. A Chem. 389 (2020) 112223.
[32] R. Mohamed, I. Mkhalid, E. Baeissa, M. Al-Rayyani, Photocatalytic degradation of methylene blue by Fe/ZnO/SiO 2 nanoparticles under visiblelight, Journal of Nanotechnology 2012 (2012).
[33] N. Yuliasari, A. Wijaya, R. Mohadi, A. Lesbani, Application of M2+ (magnesium, zinc)/alumina-metal oxide composites as photocatalysts for the degradation of cationic dyes, Ecological Engineering & Environmental Technology 23 (2022).
[34] F. Li, X. Li, C. Liu, T. Liu, Effect of alumina on photocatalytic activity of iron oxides for bisphenol a degradation, J. Hazard. Mater. 149 (2007) 199–207.
[35] S. Balamurugan, A. Balu, V. Narasimman, G. Selvan, K. Usharani, J. Srivind, M. Suganya, N. Manjula, C. Rajashree, V. Nagarethinam, Multi metal oxide

CdO–Al2O3–NiO nanocomposite—synthesis, photocatalytic and magnetic properties, Mater. Res. Express 6 (2018) 015022.
[36] F. Janani, H. Khiar, N. Taoufik, A. Elhalil, M. Sadiq, A. Puga, S. Mansouri, N. Barka, ZnO–Al2O3–CeO2–Ce2O3 mixed metal oxides as a promising photocatalyst for methyl orange photocatalytic degradation, Mater. Today Chem. 21 (2021) 100495.
[37] M. Shekhar, J. Wang, W.-S. Lee, W.D. Williams, S.M. Kim, E.A. Stach, J.T. Miller, W.N. Delgass, F.H. Ribeiro, Size and support effects for the water-gas shift catalysis over gold nanoparticles supported on model Al2O3 and TiO2, J. Am. Chem. Soc. 134 (2012) 4700–4708.
[38] F. Chen, S. Yu, X. Dong, S. Zhang, High-efficient treatment of wastewater contained the carcinogen naphthylamine by electrochemical oxidation with γ-Al2O3 supported MnO2 and sb-doped SnO2 catalyst, J. Hazard. Mater. 227–228 (2012) 474–479.
[39] X. Zhou, B. Jin, L. Li, F. Peng, H. Wang, H. Yu, Y. Fang, A carbon nitride/TiO 2 nanotube array heterojunction visible-light photocatalyst: synthesis, characterization, and photoelectrochemical properties, J. Mater. Chem. 22 (2012) 17900–17905.
[40] S. Yadav, A. Mittal, S. Sharma, K. Kumari, N.S. Chauhan, N. Kumar, Low temperature synthesized ZnO/Al2O3 nano-composites for photocatalytic and antibacterial applications, Semicond. Sci. Technol. 35 (2020) 055008.
[41] A. Sridevi, S. Krishnamohan, M. Thairiyaraja, B. Prakash, R. Yokeshwaran, Visible-light driven γ-Al2O3, CuO and γ-Al2O3/CuO nanocatalysts: synthesis and enhanced photocatalytic activity, Inorg. Chem. Commun. 138 (2022) 109311.
[42] H.B. Marulasiddeshi, P.K. Kanti, M. Jamei, S.B. Prakash, S.N. Sridhara, Z. Said, Experimental study on the thermal properties of Al2O3-CuO/water hybrid nanofluids: development of an artificial intelligence model, Int. J. Energy Res. 46 (2022) 21066–21083.
[43] D.H.A. Besisa, E.M.M. Ewais, H.H. Mohamed, Thermal performance and mechanical durability of Al2O3/CuO ceramics as solar receiver materials for solar thermal applications, Ceram. Int. 48 (2022) 23609–23617.
[44] L.-Y. Jin, M. He, J.-Q. Lu, M.-F. Luo, P. Fang, Y.-L. Xie, Comparative study of CuO species on CuO/Al2O3, CuO/CeO2-Al2O3 and CuO/La2O-Al2O3 catalysts for CO oxidation, Chin. J. Chem. Phys. 20 (2007) 582–586.
[45] C.H. Marques, A. Mesquita, V.D. Araújo, M.I.B. Bernardi, Influence of the pH on Al2O3:CuO pigments prepared by a polymeric precursor method, Mater. Res. 16 (2013).
[46] Y. Hu, C. Liu, Y. Zhang, N. Ren, Y. Tang, Microwave-assisted hydrothermal synthesis of nanozeolites with controllable size, Microporous Mesoporous Mater. 119 (2009) 306–314.
[47] K. Ocakoglu, S.A. Mansour, S. Yildirimcan, A.A. Al-Ghamdi, F. El-Tantawy, F. Yakuphanoglu, Microwave-assisted hydrothermal synthesis and characterization of ZnO nanorods, Spectrochim. Acta A Mol. Biomol. Spectrosc. 148 (2015) 362–368.
[48] M. Zawadzki, Synthesis of nanosized and microporous zinc aluminate spinel by microwave assisted hydrothermal method (microwave–hydrothermal synthesis of ZnAl2O4), Solid State Sci. 8 (2006) 14–18.
[49] M.L. Moreira, E.C. Paris, G.S. do Nascimento, V.M. Longo, J.R. Sambrano, V. R. Mastelaro, M.I. Bernardi, J. Andrés, J.A. Varela, E. Longo, Structural and optical properties of CaTiO3 perovskite-based materials obtained by microwave-assisted hydrothermal synthesis: an experimental and theoretical insight, Acta Mater. 57 (2009) 5174–5185.
[50] S.S. Ghosh, A. Sil, Porous alumina thermophotovoltaic film for output voltage enhancement of silicon solar cell at room temperature, Opt. Mater. 123 (2022) 111844.
[51] X. Liu, H. Li, C. Lu, L. Xue, Y. Yan, Optimization of ball milling process for fabrication of α-Al2O3 based coatings via laser-assisted combustion synthesis, J. Eur. Ceram. Soc. 35 (2015) 3577–3586.
[52] J. Li, Y. Wu, Y. Pan, W. Liu, Y. Zhu, J. Guo, Agglomeration of α-Al2O3 powders prepared by gel combustion, Ceram. Int. 34 (2008) 1539–1542.
[53] A. Cordier, A. Peigney, E. De Grave, E. Flahaut, C. Laurent, Synthesis of the metastable α-Al1. 8Fe0. 2O3 solid solution from precursors prepared by combustion, J. Eur. Ceram. Soc. 26 (2006) 3099–3111.
[54] Y. Tang, W. Wu, B. Wang, X. Dai, W. Xie, Y. Yang, R. Zhang, X. Shi, H. Zhu, J. Luo, Y. Guo, X. Xiang, X. Zu, Y. Fu, H2S gas sensing performance and mechanisms using CuO-Al2O3 composite films based on both surface acoustic wave and chemiresistor techniques, Sens. Actuators B 325 (2020) 128742.
[55] A. Jasim Awadh, S.H. Ammar, B.A. Altabbakh, Preparation and characteristics of CuO/γ-Al2O3 nanocomposite as efficient adsorbent for adsorption of sulfur compounds from iraqi naphtha, Mater. Today:. Proc. 42 (2021) 2596–2602.
[56] O.C. Olatunde, D.C. Onwudiwe, Selective syntheses of kuramite (Cu2SnS3) and petrukite (Cu3SnS4) phases of copper tin sulphide, and their electrochemical and photocatalytic properties, Results in Materials 13 (2022) 100249.
[57] S.D. Jackson, J.S. Hargreaves, Metal oxide catalysis, 2 volume set, John Wiley & Sons, 2008.
[58] M. Rahbar, M. Behpour, Multi-walled carbon nanotubes/TiO 2 thin layer for photocatalytic degradation of organic pollutant under visible light irradiation, J. Mater. Sci. Mater. Electron. 27 (2016) 8348–8355.
[59] S. Saravanan, R.S. Dubey, Optical and morphological studies of TiO2 nanoparticles prepared by sol–gel method, Mater. Today:. Proc. 47 (2021) 1811–1814.
[60] T. Sivanandan, S. Saravanan, Effects of calcination temperatures on structural, functional, morphological, and magnetic properties of strontium ferrite (SrFe2O4) nanoparticles, Kuwait Journal of Science 50 (2023) 271–275.
[61] A.R. Padmavathi, S.M.P.A. Das, A. Priya, T.J. Sushmitha, S.K. Pandian, S.R. Toleti, Impediment to growth and yeast-to-hyphae transition in Candida albicans by copper oxide nanoparticles, Biofouling 36 (2020) 56–72.
[62] K.K. Dey, A. Kumar, R. Shanker, A. Dhawan, M. Wan, R.R. Yadav, A.K. Srivastava, Growth morphologies, phase formation, optical & biological responses of nanostructures of CuO and their application as cooling fluid in high energy density devices, RSC Adv. 2 (2012) 1387–1403.
[63] A.F. Alamouti, M. Nadafan, Z. Dehghani, M.H.M. Ara, A.V. Noghreiyan, Structural and optical coefficients investigation of γ-Al2O3 nanoparticles using kramers-kronig relations and Z–scan technique, J. Asian Ceram. Soc. 9 (2021) 366–373.
[64] Ł. Haryński, A. Olejnik, K. Grochowska, K. Siuzdak, A facile method for tauc exponent and corresponding electronic transitions determination in semiconductors directly from UV–VIS spectroscopy data, Opt. Mater. 127 (2022) 112205.
[65] F. Aisien, N. Amenaghawon, O. Urhobotie, Potential application of a locally sourced photocatalyst for the photocatalytic decolourisation of methyl orange in aqueous solution, J. Eng. Sci. Technol 10 (2015) 1641–1653.
[66] K.A. Isai, V.S. Shrivatava, Photocatalytic degradation of methyl orange using ZnO and fe doped ZnO: a comparative study, Iranian J. Catal. 9 (2019) 259–268.
[67] A. Djebli, A. Boudjemaa, H. Bendjeffal, H. Mamine, T. Metidji, H. Bekakria, Y. Bouhedja, Photocatalytic degradation of methyl orange using ZN@[FE (CN) 5NO] complex under sunlight irradiation, Inorganic And Nano-Metal Chemistry 50 (2020) 1115–1122.
[68] R.H. Waghchaure, V.A. Adole, B.S. Jagdale, Photocatalytic degradation of methylene blue, rhodamine B, methyl orange and eriochrome black T dyes by modified ZnO nanocatalysts: a concise review, Inorg. Chem. Commun. (2022) 109764.
[69] N. Guettai, H.A. Amar, Photocatalytic oxidation of methyl orange in presence of titanium dioxide in aqueous suspension Part I: Parametric Study, Desalination 185 (2005) 427–437.
[70] M.A. Subhan, P. Chandra Saha, N. Uddin, P. Sarker, Synthesis, structure, spectroscopy and photocatalytic studies of Nano multi-metal oxide MgO•Al2O3•ZnO and MgO•Al2O3•ZnO-curcumin composite, international, J. Nanosci. Nanotechnol. 13 (2017) 69–82.
[71] S. Balamurugan, A.R. Balu, J. Srivind, K. Usharani, V. Narasimman, M. Suganya, V. S. Nagarethinam, CdOAl2O3 – a composite material with enhanced photocatalytic activity against the degradation of MY dye, Vacuum 159 (2019) 9–16.
[72] A. Mahapatra, B.G. Mishra, G. Hota, Adsorptive removal of Congo red dye from wastewater by mixed iron oxide–alumina nanocomposites, Ceram. Int. 39 (2013) 5443–5451.
[73] S. Sudhagar, S.S. Kumar, I.J.I. Premkumar, V. Vijayan, R. Venkatesh, S. Rajkumar, M. Singh, UV- and visible-light-driven TiO2/La2O3 and TiO2/Al2O3 nanocatalysts: synthesis and enhanced photocatalytic activity, Appl. Phys. A 128 (2022) 282.
[74] L.-L. Bao, Y. Li, Z. Xi, X.-Y. Wang, M. Afzal, A. Alarifi, D. Srivastava, O. Prakash, A. Kumar, J.-C. Jin, A new 2D zn (II)-based coordination polymer as photocatalyst for photodegradation of methyl orange in water: effect of photocatalyst dosage and dye concentration, J. Mol. Struct. 1292 (2023) 136103.
[75] N.F. Jaafar, A.A. Jalil, S. Triwahyono, M.N.M. Muhid, N. Sapawe, M.A.H. Satar, H. Asaari, Photodecolorization of methyl orange over α-Fe2O3-supported HY catalysts: the effects of catalyst preparation and dealumination, Chem. Eng. J. 191 (2012) 112–122.
[76] J. Cao, B. Luo, H. Lin, S. Chen, Photocatalytic activity of novel AgBr/WO3 composite photocatalyst under visible light irradiation for methyl orange degradation, J Hazard Mater 190 (2011) 700–706.
[77] A. Mahjoub, M.B. Rizi, Low temperature one-pot synthesis of cu-doped ZnO/Al2O3 composite by a facile rout for rapid methyl orange degradation, J. Photochem. Photobiol. B Biol. 175 (2017) 37–45.
[78] M. Goudarzi, M. Salavati-Niasari, Using pomegranate peel powders as a new capping agent for synthesis of CuO/ZnO/Al2O3 nanostructures; enhancement of visible light photocatalytic activity, Int. J. Hydrog. Energy 43 (2018) 14406–14416.
[79] A. Elhalil, R. Elmoubarki, M. Farnane, A. Machrouhi, F. Mahjoubi, M. Sadiq, S. Qourzal, N. Barka, Synthesis, characterization and efficient photocatalytic activity of novel Ca/ZnO-Al2O3 nanomaterial, materials today, Communications 16 (2018) 194–203.
[80] M. Chowdhury, M. Hossain, M. Azad, M. Islam, M. Dewan, Photocatalytic degradation of methyl orange under UV using ZnO as catalyst, Int. J. Sci. Eng. Res 9 (2018).
[81] L.-C. Chen, F.-R. Tsai, C.-M. Huang, Photocatalytic decolorization of methyl orange in aqueous medium of TiO2 and Ag–TiO2 immobilized on γ-Al2O3, J. Photochem. Photobiol. A Chem. 170 (2005) 7–14.